# Phase Transformations of Micron-Sized $H_2SO_4/H_2O$ Particles Studied by Infrared Spectroscopy

**Scot T. Martin, Dara Salcedo, Luisa T. Molina, and Mario J. Molina***

*Department of Chemistry and Department of Earth, Atmospheric, and Planetary Sciences, Massachusetts Institute of Technology, Cambridge, Massachusetts 02139*

*Received: February 18, 1997; In Final Form: April 30, 1997*[⊗]

A new experimental technique has been developed for investigations of phase transitions of micron-sized particles through infrared spectroscopy. The particles are attached to the inner walls of a gold light pipe, enabling long observation times, temperature cycling, regulation of the particle composition, and statistically significant sampling (i.e., large particle populations). Phase transitions of 5−10 $\mu$m particles with compositions ranging from 10 to 60 wt % sulfuric acid in water have been studied with this technique. The results are in agreement with expectations in terms of (1) the dependency of light scattering upon particle size, (2) the extent of water uptake as monitored by the infrared spectra, (3) the formation of ice and sulfuric acid tetrahydrate (SAT), and (4) the equilibrium melting temperatures of these solids. In agreement with previous studies on the $H_2SO_4/H_2O$ system employing relatively large liquid volumes, the micron-sized droplets with compositions in the range from 40 to 60 wt % form glasses upon cooling; however, these droplets do not crystallize upon warming, in contrast to the observed behavior of the larger samples.

## Introduction

Polar stratospheric clouds (PSCs) catalyze key reaction steps in the annual process of polar ozone destruction.[1] PSCs form from the background sulfuric acid aerosol in the stratosphere as the temperature falls in the polar winter and the particles absorb water and nitric acid to form supercooled liquid ternary solutions (STS). These liquid aerosols are metastable with respect to the formation of several solid phases, including sulfuric acid tetrahydrate (SAT) and nitric acid trihydrate (NAT). Recent laboratory experiments indicate that solid phase formation from STS does not occur until the ice frost point is reached.[2−4] Field observations, however, appear to suggest that solid phases are present in air parcels that have not reached temperatures below the ice frost point;[5] on the other hand, the role of temperature fluctuations might have been overlooked.[6] Additional laboratory and field studies are clearly needed to resolve the discrepancy.[2−4,7−12]

One problem for laboratory experiments is to provide an accurate simulation of atmospheric processes. Two approaches are commonly employed: in the first one, the freezing behavior of ternary liquid solutions contained in test tubes is investigated.[2,13] In this case, the volume of liquid is typically $10^{12}$ times larger than that of atmospheric aerosols. Furthermore, freezing statistics are difficult to obtain due to the stochastic nature of nucleation. In the second approach, the freezing behavior of liquid aerosols suspended in a cooled chamber is investigated.[4,14] In this case, observation times comparable to atmospheric time scales are not practical due to particle sedimentation; in addition, the uncertainty in the liquid aerosol composition is often large because it is difficult to establish when the particles have reached equilibrium with the gas phase. Furthermore, temperature cycling representative of atmospheric phenomena is difficult to simulate due to the slow heating and cooling rates that are practical for chambers.

In this paper, we describe a new experimental approach for the observation of the freezing behavior of small liquid droplets. Several advantages of this new approach include the possibilities for long observation times, the capability to carry out temperature cycling, an extended temperature range (from 300 to 130 K), the regulation of particle composition through equilibration with the gas phase, and reliable freezing statistics for large particle ensembles. This new technique is employed here to investigate 5−10 $\mu$m sulfuric acid particles of varying composition from 10 to 60 wt %. The particles are deposited on the inner walls of a gold-coated light pipe, and their composition is regulated by controlling the partial pressure of $H_2O$ vapor (i.e., relative humidity). Phase transitions accompanying changes in temperature are monitored by infrared spectroscopy. A limitation of this technique is that the gold surface inside the sample cell may initiate heterogeneous freezing of the particles. In fact, it appears that gold induces the formation of water−ice crystals; hence, we report the freezing temperatures to form ice as upper limits. On the other hand, there is a wide range of compositions for which no freezing takes place, and we find that the freezing behavior of small liquid sulfuric acid droplets in some cases is qualitatively different from expectations based upon the freezing behavior of larger volumes. In a subsequent paper, we will report the results of freezing studies of $H_2SO_4/HNO_3/H_2O$ droplets which simulate polar stratospheric cloud particles.

## Experimental Section

**General Description.** The flow chart for the procedure to deposit small liquid particles into the sample cell and the schematic diagram of the experimental apparatus are shown in Figures 1 and 2, respectively. The sample cell consists of a gold-coated stainless steel tube (6.3 mm o.d., 4.8 mm i.d., 30 cm long) with a mirrorlike inner surface ($\sim 3 \times 10^{-5}$ cm rms); the two ends are sealed with AgCl windows. In a typical experiment, a liquid in the reservoir is pumped to a nebulizer where a spray of small particles is generated, a fraction of which deposits on the inner walls of the sample cell. The cell is then inserted into the cooling stage and connected to the gas lines. The relative humidity (RH) inside the cell is controlled by the continuous flow of a mixture of dry $N_2$ and humidified $N_2$; it is

* To whom correspondence should be addressed.
[⊗] Abstract published in *Advance ACS Abstracts,* June 15, 1997.

S1089-5647(97)00607-X CCC: $14.00 

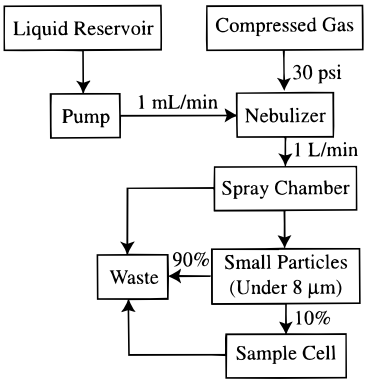


**Figure 1.** Flow chart for the procedure to generate aerosol and to deposit the particles on the walls of the sample cell.

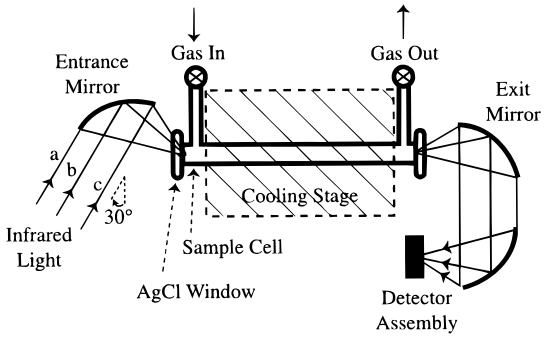


**Figure 2.** Schematic diagram of the FTIR experimental apparatus. Light rays a−c are discussed in the text.

measured downstream of the cell by a solid-state hygrometer. The relative humidity within the cell is regulated via the gas flow for 30 min to adjust the particle composition at room temperature; subsequently, the gas valves are sealed. The cell is then cooled in steps of 5 or 10 K and held at each temperature for 5 min before an infrared spectrum is recorded. The step size and rate are similar for warming. In the freezing rate experiments, the temperature is held constant while infrared spectra are recorded as a function of time. Note that these freezing experiments are carried out essentially at constant droplet composition, whereas in the atmosphere the process occurs at constant water partial pressure, and hence the composition of the liquid droplets changes with temperature.

**Particle Generation and Deposition.** The nebulizer (Meinhard, TR-30) is operated at a liquid flow rate of 1 mL $min^{-1}$ and at a gas flow rate of 1 L $min^{-1}$, which corresponds to 30 psig of $N_2$. The spray chamber (Meinhard) is an impactor that collects particles above 8 $\mu$m under the specified operating conditions. As shown in Figure 1, the flow from the spray chamber is divided so that only 100 mL $min^{-1}$ flow through the sample cell. The flow velocity is $\sim$2 cm $s^{-1}$, which yields an average residence time of 15 s inside the cell. The Reynolds number is 7 (i.e., laminar flow conditions). In order to deposit particles only along the central 23 cm of the sample cell, 3.8 cm Teflon sleeve inserts are inserted at each end of the cell prior to particle deposition and are removed afterward. This step is important so that all deposited particles are contained within the cooling stage (see Figure 2). All materials that the aerosol comes into contact with are made from glass, Teflon, or gold.

For a typical loading, the particles are vented for the first minute, bypassing the sample cell, in order to form a homogeneous particle field. Next, 10% of the flow is directed through the sample cell for 1 min. The flow is then redirected to bypass the cell for another 1.5 min, and the cell is rotated by one-quarter turn. The loading process is then repeated for three more rotations. The resulting deposition inside the cell is radially and longitudinally symmetric to yield particles that cover $\sim$10% of the surface area. The particle diameters vary from 5−10 $\mu$m for 10 wt % to 25 $\mu$m for 60 wt %. The laminar flow conditions in the cell and the necessity to rotate the cell indicate that the particles deposit to some extent through sedimentation; the fall velocity for a 10 $\mu$m sphere at 1 atm pressure is 3 mm $s^{-1}$.[15]

**Particle Size Characterization.** A thin-walled glass tube is substituted for the sample cell. After particle deposition, the glass tube is observed at 400$\times$ magnification with an optical microscope. The particle generation and deposition methodology for obtaining a radially and longitudinally symmetric deposition of particles that cover 10% of the surface area was developed by employing this approach of visual characterization. The assumption is made that deposition on the surfaces of the glass tube is similar to that on the gold surface; it is likely that the "sticking" coefficient for the liquid droplets is close to unity on both surfaces. Furthermore, the infrared spectrum in the sample cell clearly differentiates between well-separated particles and coalescing particles; it appears that in the former case the spectrum is a combination of the real and imaginary components of the refractive index, whereas it is dominated by the real component in the latter case.

**Cooling Stage.** The experimental apparatus for the control of temperature and gas-phase composition and for infrared spectroscopy is shown schematically in Figure 2. The sample cell is placed inside a cooling stage machined from a single block of aluminum and enclosed in polyurethane foam insulation. The temperature is controlled by constant cooling provided by a liquid nitrogen reservoir counterbalanced by four resistive heaters coupled to a temperature controller (Omega CN76022). The temperature is measured with several type T thermocouples placed near the heaters and directly next to the sample cell through small holes drilled into the aluminum block. The thermocouples are individually calibrated and are accurate to within $\pm$1 K. The apparatus has a maximum cooling rate from 295 to 200 K of 30 min and maximum warming rate from 200 to 295 K of 10 min. The apparatus reaches a minimum temperature of 130 K after 1 h. At 200 K, the temperature gradient within the sample cell is $<$1 K from end to end. After a new set point temperature is reached, the cooling stage requires $\sim$5 min for all of the thermocouples to reach the same value. The entire sample holder is placed within a purged acrylic box to remove $CO_2$ and $H_2O$ for the infrared measurements.

**Infrared Measurements.** A Nicolet 800 FTIR equipped with a MCT-A detector is used to collect infrared spectra. A typical spectrum is recorded at 16 $cm^{-1}$ resolution with 256 scans. The transmission spectrum is obtained by taking the ratio of the spectrum of the loaded sample cell against the spectrum of an empty and flushed cell. The irradiation geometry is shown in Figure 2. The collimated infrared beam is focused by a gold-plated off-axis parabolic mirror into the entrance of the sample cell. A maximum in the signal-to-noise ratio of the infrared spectra is obtained by placing the cell at 30° angle relative to the input beam. The light cone exiting from the cell is collected by a second off-axis parabolic mirror and directed to the detector assembly. Calculations based upon ray optics and omitting any effects due to light scattering by the particles indicate that rays a, b, and c when entering the cell through its radial center reflect 17, 36, and 84 times, respectively, before exiting the cell. Similar rays when entering at 50% off-axis reflect 20, 42, and 97 times, respectively, and at 80% off-axis reflect 32, 68, and 160 times.

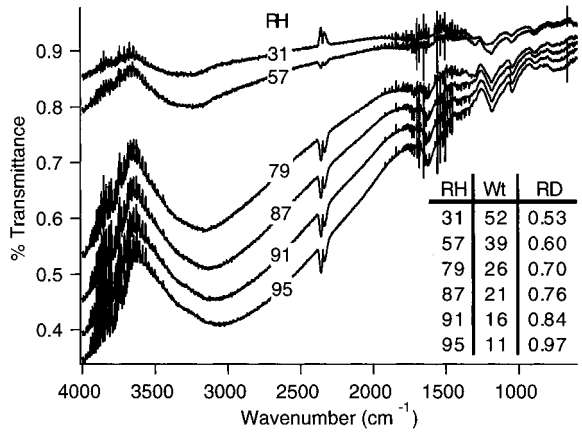


**Figure 3.** Infrared spectra at 295 K of sulfuric acid particles equilibrated at different relative humidities. Inset: RH is the relative humidity, Wt is weight percent composition of an equilibrated sulfuric acid solution, and RD is the calculated relative diameter of a spherical particle composed of a constant sulfuric acid content and a varying water content, with RD ≡ 1.00 for 10 wt % composition.

## Results

The infrared spectra of a single set of sulfuric acid particles equilibrated in steps from 31 to 95% relative humidity (RH) at 295 K are shown in Figure 3. The spectra are not offset from one another. In the spectral region 1000−4000 $cm^{-1}$, the slope in the base line increases with RH. Whereas the band positions at 1184, 1045, and 891 $cm^{-1}$ appear to be independent of RH, the band intensities increase monotonically with RH. The spectra are reproducible whether the target RH is approached from the dry or wet directions. In these spectra, gas-phase water absorption is removed by spectral subtraction. The residual gas-phase water shown in the spectra indicates the limits of the spectral subtraction and arises from the pressure dependency of the water vapor spectrum.

The initial aerosol composition in Figure 3 is 10 wt % before the adjustment of the relative humidity altered the particle composition, as shown in the inset of Figure 3. The relation between relative humidity of water and the composition of the sulfuric acid droplets is calculated according to the thermodynamic model of Carslaw et al.[16] The diameter, $d$, of the particles is calculated as follows:

$$d^3 = \frac{6}{\pi} V = \frac{6}{\pi} m\rho = \frac{6}{\pi} \frac{m_s}{w} \rho \qquad (1)$$

where $V$ is the volume of the particle, $m$ is the mass, $\rho$ is the density, $w$ is the sulfuric acid weight fraction composition, and $m_s$ is the mass of sulfuric acid in the particle. The relative diameter, RD, is the ratio of the diameter of a particle of composition $x$% to the diameter of a particle composed of 10 wt % sulfuric acid. The relative diameters are given in the figure inset and are calculated as follows:

$$\mathrm{RD} \equiv \frac{d_{x\%}}{d_{10\%}} = \left( \frac{(10\%)\rho_{x\%}}{(x\%)\rho_{10\%}} \right)^{1/3} \qquad (2)$$

The infrared spectra of 20 wt % $H_2SO_4$ particles at 294 and 246 K from 800 to 1300 $cm^{-1}$ are shown in Figure 4a. At 294 K, infrared absorptions are observed at 1180, 1049, and 887 $cm^{-1}$. These features arise from $HSO_4^-$.[17] However, at 246 K, the $HSO_4^-$ bands weaken and become shoulders, and a new band at 1103 $cm^{-1}$ from $SO_4^{2-}$ appears. The thermodynamic calculation of percent speciation of $H_2SO_4$ as $SO_4^{2-}$ as a function of composition at several temperatures is shown in Figure 4b,

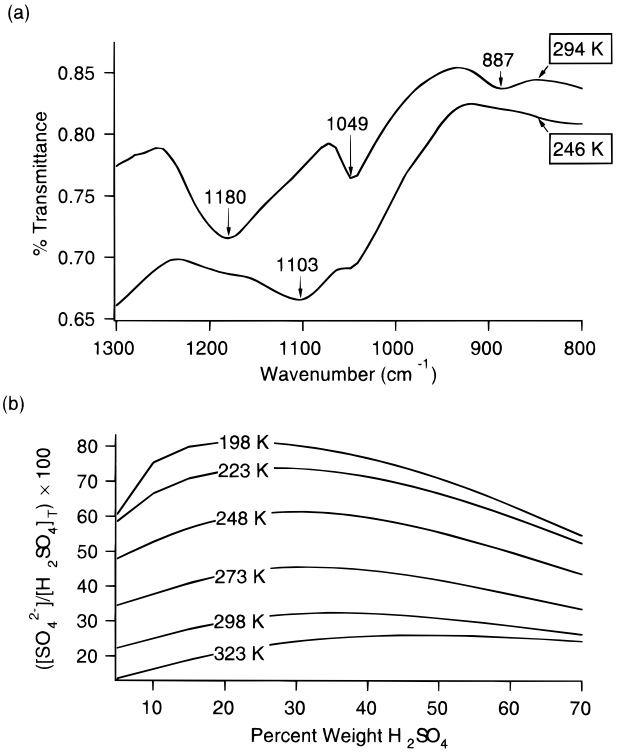


**Figure 4.** (a) Infrared spectra of 20 wt % $H_2SO_4$ particles at 294 and 246 K. The spectra are offset for clarity. (b) Calculated percent speciation of $H_2SO_4$ as $SO_4^{2-}$ versus composition at several temperatures (kelvin); $[H_2SO_4]_T = [SO_4^{2-}] + [HSO_4^-]$.

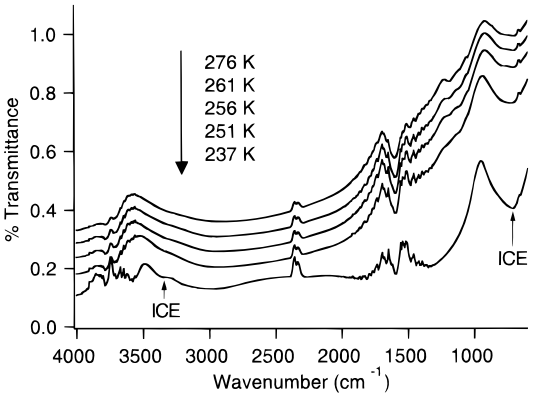


**Figure 5.** Infrared spectra of 10 wt % $H_2SO_4$ particles at different temperatures, obtained during cooling. The spectra are offset for clarity.

where $[H_2SO_4]_T = [SO_4^{2-}] + [HSO_4^-]$. The figure shows that percent $SO_4^{2-}$ increases as temperature decreases;[18] the general dependence of percent $SO_4^{2-}$ on weight percent composition agrees with laboratory measurements carried out at 298 K.[19] The calculations are performed using the thermodynamic model of Carslaw et al.[16]

The infrared spectra of 10 wt % $H_2SO_4$ particles undergoing cooling from 276 to 237 K are shown in Figure 5. Cooling is carried out in steps of 5 K. The first changes in the spectra occur at 251 K, and the shoulders from 3000 to 3500 $cm^{-1}$ and the peak at 800 $cm^{-1}$ indicate ice formation.[20] Further ice formation is observed as the temperature drops to 237 K.

The infrared spectra of 30 wt % $H_2SO_4$ particles undergoing cooling and warming cycles from 220 to 180 K are shown in Figure 6. The sample cell is cooled in steps of 5 K and equilibrated at each new temperature for 5 min. The first spectral changes during cooling are observed at 189 K, as shown in Figure 6a. Ice formation is indicated by the shoulders between 3000 and 3500 $cm^{-1}$ and the peak at 800 $cm^{-1}$,[20] and

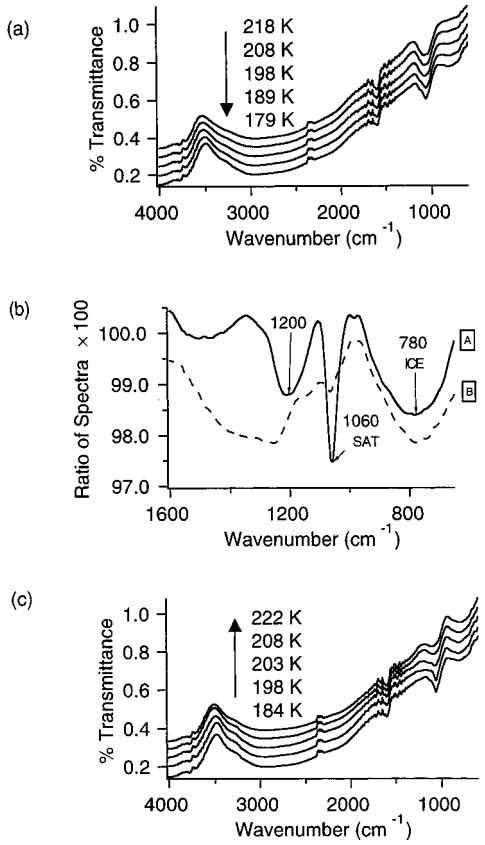


**Figure 6.** Infrared spectra of 30 wt % $H_2SO_4$ particles. The spectra are offset for clarity. (a) Transmittance spectra obtained during cooling at different temperatures. (b) Trace A: ratio spectrum calculated by dividing the transmittance spectrum at 189 K by the one at 198 K. Trace B: ratio spectrum calculated by dividing the 198 K spectrum by the one at 208 K. (c) Transmittance spectra at several temperatures obtained during warming.

SAT formation is apparent by the sharp peak at 1060 $cm^{-1}$.[18] Further formation of ice and SAT occurs at 179 K. A separate experiment (not shown in Figure 6) indicated that the spectra of 30 wt % particles held at 189 K continue to change for 60 min before the formation of ice and SAT is complete.

The ratio of two consecutive transmittance spectra makes spectral changes more apparent, as shown in Figure 6b for the spectral region from 700 to 1600 $cm^{-1}$: trace B is the ratio of the spectrum taken at 198 K to the one at 208 K, which is considered as the background. In this case, the ratio spectrum is interpreted as a percent transmittance, and downward peaks indicate the formation of a new species. Spectrum A in Figure 6b thus shows the formation of SAT at 189 K by the presence of a sharp band at 1060 $cm^{-1}$. The formation of ice is indicated by the spectral feature at 780 $cm^{-1}$. The change at 1200 $cm^{-1}$ arises from a shift in the speciation of $SO_4^{2-}/HSO_4^-$ due to the combined effects of changes in temperature and in liquid phase composition. Spectrum B, on the other hand, indicates that SAT formation is not occurring at 198 K.

Spectral changes upon the warming of 30 wt % $H_2SO_4$ particles begin at 203 K, as shown in Figure 6c. The first changes occur as the loss of the sharp peak at 1060 $cm^{-1}$ and the growth of a broad peak at 1100 $cm^{-1}$, which is consistent with the melting of SAT to form a $H_2SO_4/H_2O$ liquid solution. The eutectic for this system occurs at 200 K. The shoulders from 3000 to 3500 $cm^{-1}$ and the band at 800 $cm^{-1}$ indicate that ice is still present in the system at 222 K. The decrease in band intensities for ice (3000−3500 $cm^{-1}$) between 203 and 222 K, however, shows that the ice has partially melted. The spectral evidence in this region thus indicates that the particles

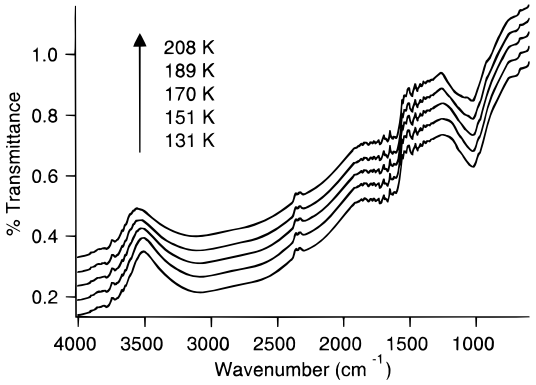


**Figure 7.** Infrared spectra of 50 wt % $H_2SO_4$ particles at different temperatures, obtained during warming. The spectra are offset for clarity.

exist as solid/liquid mixtures in this temperature range. A comparison of the spectra in Figure 6a,c demonstrates the occurrence of supercooling for the 30 wt % $H_2SO_4$ particles.

The infrared spectra of 50 wt % $H_2SO_4$ particles undergoing warming from 131 to 208 K are shown in Figure 7. Warming is carried out in steps of 10 K. The spectra taken at 131 and 151 K are identical, and the small shifts associated with the $HSO_4^-/SO_4^{2-}$ temperature-dependent equilibrium do not occur.[18] The inhibition of proton exchange suggests that the particles form a solid solution (i.e., a glass).[21] Upon further warming from 170 to 208 K, spectral shifts appear in the region from 800 to 1200 $cm^{-1}$ that indicate a temperature-dependent equilibrium between $HSO_4^-$ and $SO_4^{2-}$ and thus suggest a liquid is present. No sharp peak at 1060 $cm^{-1}$ is apparent during the warming process, and thus the formation of SAT upon warming does not appear to occur for these particles.

The identities of the phases observed by infrared spectroscopy upon the cooling and warming of $H_2SO_4$ particles at various temperatures and liquid-phase compositions are shown in Figure 8. The method of ratios is employed in order to determine the onset temperature of freezing and the final temperature of melting. The squares represent the initial compositions of the particle at 298 K, which remains unchanged as long as no solid phase is present. The phase diagram showing the temperatures and liquid phase compositions at which ice, SAT, and sulfuric acid semihexahydrate (SAH) are in equilibrium with the liquid phase[22] is superimposed in Figure 8.

The phases observed upon cooling are shown in Figure 8a. Ice is first observed at 251 and 241 K upon cooling 10 and 20 wt % $H_2SO_4$ particles; the equilibrium temperatures are 268 and 258 K, respectively. Supercooling of 17 K is thus observed for these two cases. At 30 wt %, SAT formation is first observed at 194 K. In this case, ice forms between 227 and 190 K, but it is not possible to measure the actual onset temperature of freezing because of the small amount of ice formed, as expected from the lever rule. For compositions from 40 to 60 wt %, nucleation of neither ice nor SAT is observed. An amorphous glass appears to form below 150 K.

The phases observed upon warming the $H_2SO_4$ particles are shown in Figure 8b. For 10, 20, and 30 wt %, ice melts at 268, 263, and 234 K, respectively. The uncertainty of for these melting temperatures corresponds to the 5 K step size of the warming process. Within that limit, the melting temperatures agree with the values obtained from the phase diagram, namely, 268, 258, and 237 K, respectively. SAT is observed to melt at 203 K upon warming the 30 wt % composition; the eutectic occurs at 201 K. For 40−60 wt %, all changes in the infrared spectra are consistent with the temperature-dependent equilib-

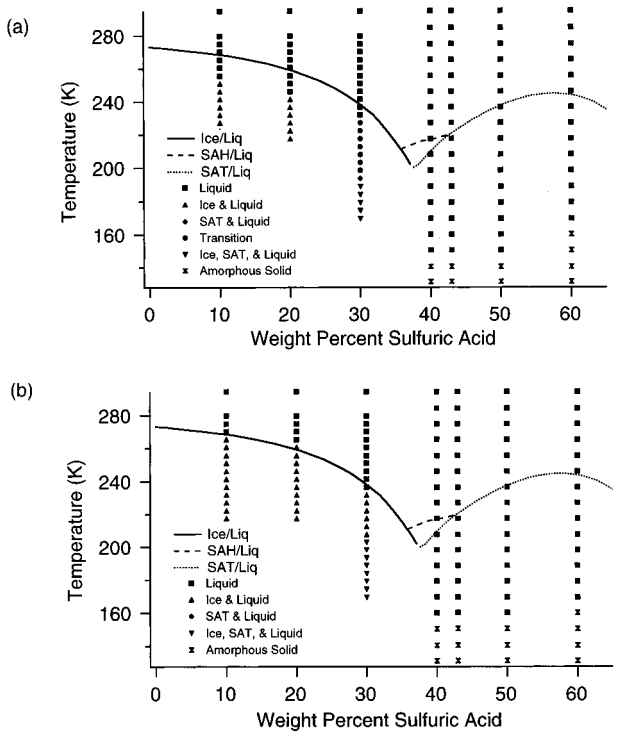


**Figure 8.** Identity of phases observed upon (a) cooling and (b) warming $H_2SO_4$ particles as a function of temperature and liquid-phase composition. The sulfuric acid/water equilibrium freezing temperatures obtained from Gable et al.[22] are superimposed as lines (SAH = hemihexahydrate; SAT = tetrahydrate).

rium between $HSO_4^-$ and $SO_4^{2-}$. Nucleation of solids, including SAT, is not observed between 40 and 60 wt %.

To evaluate the role of the gold-coated sample cell as a surface for heterogeneous nucleation, several test tube experiments were carried out as described by Beyer et al.[13] and Koop et al.[2] In the case of 20 and 25 wt % $H_2SO_4$, the observed freezing temperature in the presence of a section of the sample cell was 5 K higher than in the absence of the sample cell for three replicate measurements. The sample cell thus appears to provide a surface for heterogeneous nucleation of ice. In the absence of the sample cell, supercooling of 20 K is observed at 20 and 25 wt %.

## Discussion

**Particle Composition.** A meaningful interpretation of the phase transitions presented in Figures 3−8 requires a knowledge of the chemical composition of the particles in the sample cell. First, the agreement between the observed and expected melting temperatures over the range of compositions shown in Figure 8b suggests that the expected acid composition is indeed obtained by the equilibration procedure. Second, the spectra recorded in Figure 3 for the adjustment of particle composition by relative humidity are identical whether the relative humidity is approached from above or below. This fact again suggests that the particles do attain the expected equilibrium composition.

In principle, water vapor condensing into the particles upon cooling could change their chemical composition. However, a calculation indicates that the condensed-phase mass exceeds the water vapor mass by at least a factor of 20; thus, the condensation of the vapor yields a negligible change in the particle composition. The calculation is based upon a 10% surface coverage of the sample cell by 10 $\mu$m particles formed as spheres in an atmosphere of $2.03 \times 10^{-2}$ atm of water (88% RH to yield 20 wt % $H_2SO_4$ particles at 20 °C) using the following information: cell surface area, $A = 34$ cm$^2$; cell volume, $V = 4$ cm$^3$; particle cross section, $\sigma = 7.9 \times 10^{-7}$ cm$^2$ per particle; number of particles, $N = 0.1\ A/s = 4.3 \times 10^6$ particles; density of particles, $\rho = 1$ g/cm$^3$; particle mass, $m = (4/3)\pi r^3\rho = 5.2 \times 10^{-10}$ g per particle; total mass of particles, $M_p = Nm = 2.3$ mg; and total vapor-phase mass of water, $M_v = PV(\mathrm{MW})/RT = 61$ $\mu$g. The ratio of $M_p$:$M_v$ is thus 38 for 20 wt % $H_2SO_4$. Full condensation of the water should shift the composition by ∼0.5 wt % from 20 to 19.5 wt %. For higher percent weight compositions, the ratio $M_p$:$M_v$ increases further because the equilibrium partial pressure of $H_2O$ decreases. These calculations and the empirical observations cited above both suggest that the procedure followed for the deposition and equilibration of the particles yields the expected chemical composition over the range of temperatures studied.

**Light Scattering.** The sloping base line in Figures 3−7 arises from light scattering by particles in the sample cell. As RH increases from 31 to 95% in Figure 3, the particle size approximately doubles, and the slope of the base line increases by 4-fold. Mie theory provides a qualitative description of this and suggests that maximum light scattering should occur when the particle radius approximately equals the wavelength of light.[23] In the case of Figure 3, RD = 1.00 corresponds to 5−10 $\mu$m or 2000−1000 cm$^{-1}$. However, the complicated optical geometry makes a quantitative model impractical. In principle, though, it should be possible to adapt algorithms that calculate Mie scattering so that particles can be sized based upon the scattering component of the infrared spectrum observed in the sample cell.

In Figures 4−7, the slope of the base line does not change during temperature cycling, which suggests that the particle size and shape remain constant during cooling and warming. This observation is also consistent with the aforementioned calculation that there is insufficient water vapor in the system to perturb the particle size or composition upon cooling.

**Spectral Features.** Scattering and reflection in the sample cell shift the infrared spectral bands of the supported particles by up to 20 cm$^{-1}$ as compared to simple transmission measurements.[24] Shifted bands arise in the sample cell because both the real and imaginary parts of refractive index contribute to the infrared spectrum. In Figure 4a, for example, bands arising from $HSO_4^-$ occur at 1180, 1049, and 887 cm$^{-1}$. These features are commonly reported at 1190, 1050, and 880 cm$^{-1}$ in transmission spectra that measure the imaginary part of the refractive index.[25] Though shifted in some cases, the bands observed in Figures 4−7 for ice, SAT, $HSO_4^-$, and $SO_4^{2-}$ are all in qualitative agreement with literature assignments with respect to band shape, patterns, and location.

In addition to the band shifts, several other interesting spectral features are also apparent. First, in Figure 3, the band intensities increase with relative humidity. This effect probably occurs because of the larger surface area coverage by the particles. For example, for RH = 95%, the surface coverage is 10% so that a typical input beam (ray b), which reflects ∼36 times in the sample cell, is expected to interact with the particles three times. For RH = 31%, surface coverage is 3% due to the reduced particle size, and the typical beam thus interacts only once with the particles. In this case, the spectral intensities recorded at RH = 95 should be 3 times those recorded at RH = 31, which is in qualitative agreement with the observations in Figure 3.

A second interesting spectral feature is the temperature dependence shown in Figure 4a. The temperature dependence of the equilibrium between $HSO_4^-$ and $SO_4^{2-}$ has been reported previously.[18] At 294 K, the spectrum indicates the liquid composition is predominantly $HSO_4^-$. This composition is

consistent with the speciation of 30% $SO_4^{2-}$ and 70% $HSO_4^-$, as shown in Figure 4b for 20 wt % $H_2SO_4$ at 294 K. At 246 K, the infrared spectrum in Figure 4a indicates that the liquid composition changes, yielding approximately equal parts of $HSO_4^-$ and $SO_4^{2-}$. The calculations presented in Figure 4b suggest that the liquid composition should be 60% $SO_4^{2-}$ and 40% $HSO_4^-$ under these conditions. The general shift from $HSO_4^-$ to $SO_4^{2-}$ is seen in Figure 7 above 151 K; below this temperature, the spectrum remains unchanged. This effect appears to result from the formation of an amorphous solid or glass that thus hinders further proton exchange between $HSO_4^-$ and $SO_4^{2-}$.

**Phase Transitions.** Dilute sulfuric acid particles, from 0 to 35 wt % with a radius of 0.2 $\mu$m, have been reported to supercool by 40 K.[26] More concentrated particles, from 40 to 60 wt %, are known to supercool even more deeply.[4] Although in our experiments the particles above 40 wt % supercool deeply in the sample cell, the more dilute particles from 10 to 30 wt % supercool by only 20 K, as shown in Figure 8a. Because these particles are 5−10 $\mu$m, it is possible that the rate of homogeneous nucleation has increased relative to the 0.2 $\mu$m particles so that a supercooling of only 20 K is observed. Indeed, in the test tube experiments on bulk volumes, 20 K supercooling is observed. However, a more likely explanation for the reduced supercooling is that heterogeneous nucleation of ice occurs on the gold-coated walls. This explanation is consistent with the observation that the sample cell acts as a heterogeneous nucleation center in the test tube experiments. In this case, the results reported in Figure 8a represent an upper limit for homogeneous freezing temperatures. In ongoing work in the laboratory, we are modifying the coating process of the sample cell in an effort to obviate heterogeneous nucleation.

Whether homogeneously or heterogeneously, once ice formation occurs for compositions of less than 37.5 wt % $H_2SO_4$, further cooling should yield the continued formation of ice and a shift in the liquid to more concentrated solutions. This result is shown in Figure 5: after the initial ice formation at 251 K, additional ice formation is observed as the temperature drops. Freezing rate experiments, however, show that when holding the temperature constant, freezing is not complete even after 60 min. In the cooling experiments, the rate of cooling is 0.5 K/min. Thus, the observed spectral changes upon cooling appear to be a combination of effects from the lever rule and from kinetics. The persistence of liquid below the eutectic temperature in Figure 8a for 30 wt % is thus best understood as a kinetic effect. In fact, kinetic experiments in this region show complete freezing after 60 min.

**Comparison with Previous Work.** Several experiments on the phase transitions of binary sulfuric acid drops have been reported.[3,4,26,27] Bertram et al.,[26] studying 0.2 $\mu$m particles with $H_2SO_4$ compositions lower than 35 wt %, find that these particles supercool 35 K with respect to the liquid−ice equilibrium temperature before freezing to form ice. Anthony et al.,[3] studying sulfuric acid aerosols with $H_2SO_4$ compositions greater than 35 wt % (ca. 0.5 $\mu$m diameter), do not find freezing in the range 189−240 K. Clapp et al.,[20] conducting experiments with compositions ranging from 25 to 85 wt % sulfuric acid, find that particles more acidic than 40 wt % do not freeze at temperatures as low as 160 K, whereas particles less acidic than 35 wt % form ice at temperatures 20−40 K below the freezing temperature. Furthermore, Clapp et al. state that ice formation does not cause the whole drop to freeze. Instead, two phases (ice and sulfuric acid liquid) are present until the sulfuric acid octahydrate forms below 180 K. Qualitatively, all of these results agree with those reported in this paper. Quantitatively, however, the supercooling reported by Anthony et al. and Clapp et al. of aerosol drops consisting of less than 35 wt % $H_2SO_4$ is 20 K colder than observed in our experiments. This result supports our conclusion that the gold surface of the sample cell induces heterogeneous freezing of ice.

In a single drop experiment, Imre et al. find that a drop following the ice/liquid coexistence curve remains liquid until 166 K and then crystallizes after 4−5 h to form sulfuric acid octahydrate.[27] In our experiments no crystal formation is observed under similar conditions (i.e., 45 wt % at 166 K), as shown in Figure 8a. However, we hold the temperature between 160 and 170 K for only 10 min in the present experiments before cooling to the next temperature step.

Previous workers have observed that the warming of an amorphous glass formed by sulfuric acid solutions above 40 wt % leads to the nucleation of SAT.[21,18] In the particle experiments described here, however, no nucleation is observed during warming from 130 K, as shown in Figures 7 and 8b. The apparent implication is that the formation of SAT germs in the glass is sparse. In a bulk sample, these sparse germs are able to grow and hence yield the complete freezing of the entire sample. However, the probability of occurrence of a germ in an individual micron-sized particle appears to be small. It is likely that several particles contain SAT germs and freeze, but the fraction appears to be small, since no SAT is detected in the infrared spectrum. In this case, the extrapolation from the freezing behavior of bulk volumes to small particles is not valid.

## Conclusions

A new technique has been developed for the study of the freezing behavior of micron-sized liquid droplets. In contrast to the limitations of previous techniques, the new apparatus enables long observation times, temperature cycling, regulation of the particle composition, and statistically significant experiments (i.e., large sample populations). The generation and deposition of the small particles, the equilibration procedure to control their composition, and the optical arrangement for infrared spectroscopy are reasonably well validated by observations of the dependence of light scattering upon particle size, of water uptake in the infrared spectra, of ice and SAT formation, and by the agreement between the observed and expected melting temperatures based upon the water/sulfuric acid phase diagram. Ice nucleates heterogeneously on the gold surface inside the sample cell; however, SAT and other hydrates do not nucleate on the cell surfaces. Once formed, the ice provides a surface that nucleates SAT. A similar process may take place after the formation of type II PSCs during the polar winter. In contrast to previous studies on the water/sulfuric acid system employing large liquid volumes, small droplets do not nucleate SAT readily from supercooled glasses upon warming. Therefore, the extrapolation of freezing behavior from large volumes of liquids to small droplets is not appropriate in this case. The freezing behavior of small ternary liquid droplets simulating polar stratospheric cloud particles is now being investigated in our laboratory using this new apparatus.

**Acknowledgment.** The research described in this article is supported by a grant from NASA's Atmospheric Effects of Aircraft Program. S.T.M. is a NOAA Postdoctoral Fellow in Climate and Global Change. Support for D.S. was obtained from DGAPA at the Universidad Nacional Autonoma de Mexico. Technical assistance from Dora Farkas is also appreciated.

## References and Notes

(1) World Meteorological Organization. *Scientific Assessment of Ozone Depletion: 1994*; WMO Global Ozone Research and Monitoring Project, Report No. 37; 1994.

(2) Koop, T.; Biermann, U. M.; Raber, W.; Luo, B. P.; Crutzen, P. J.; Peter, T. *Geophys. Res. Lett.* **1995**, *22*, 917.

(3) Anthony, S. E.; Onasch, T. B.; Tisdale, R. T.; Disselkamp, R. S.; Tolbert, M. A.; Wilson, J. C. *J. Geophys. Res.*, submitted for publication.

(4) Clapp, M. L.; Niedziela, R. F.; Richwine, L. J.; Dransfield, T.; Miller, R.; Worsnop, D. R. *J. Geophys. Res.*, in press.

(5) Larsen, N.; Knudsen, B. M.; Rosen, J. M.; Kjome, N. T.; Kyrö, E. *Geophys. Res. Lett.* **1996**, *23*, 1091.

(6) Meilinger, S. K.; Koop, T.; Luo, B. P.; Hutwelker, T.; Carslaw, K. S.; Krieger, U.; Crutzen, P. J.; Peter, T. *Geophys. Res. Lett.* **1995**, *22*, 3031.

(7) Molina, M. J.; Zhang, R.; Wooldridge, P. J.; Mcmahon, J. R.; Kim, J. E.; Chang, H. Y.; Beyer, K. D. *Science* **1993**, *261*, 1418.

(8) Fox, L. E.; Worsnop, D. R.; Zahniser, M. S.; Wofsy, S. C. *Science* **1995**, *267*, 351.

(9) Tabazadeh, A.; Toon, O. B. *J. Geophys. Res.* **1996**, *101*, 9071.

(10) Tabazadeh, A.; Toon, O. B.; Gary, B. L.; Bacmeister, J. T.; Schoeberl, M. R. *Geophys. Res. Lett.* **1996**, *23*, 2109.

(11) Tolbert, M. A. *Science* **1996**, *272*, 1597.

(12) Tolbert, M. A. *Science* **1994**, *264*, 527.

(13) Beyer, K. D.; Seago, S. W.; Chang, H. Y.; Molina, M. J. *Geophys. Res. Lett.* **1994**, *21*, 871.

(14) Disselkamp, R. S.; Anthony, S. E.; Prenni, A. J.; Onasch, T. B.; Tolbert, M. A. *J. Phys. Chem.* **1996**, *100*, 9127.

(15) Seinfeld, J. H. *Atmospheric Chemistry and Physics of Air Pollution*; Wiley: New York, 1986.

(16) Carslaw, K. S.; Clegg, S. L.; Brimblecombe, P. *J. Phys. Chem.* **1995**, *99*, 11557.

(17) Giguère, P. A.; Savoie, R. *J. Am. Chem. Soc.* **1963**, *85*, 287.

(18) Zhang, R.; Wooldridge, P. J.; Abbatt, J. P. D.; Molina, M. J. *J. Phys. Chem.* **1993**, *97*, 7351.

(19) Dawson, B. S. W.; Irish, D. E.; Toogood, G. E. *J. Phys. Chem.* **1986**, *90*, 334.

(20) Clapp, M. L.; Miller, R. E.; Worsnop, D. R. *J. Phys. Chem.* **1995**, *99*, 6317.

(21) Vuillard, G. *Soc. Chim.—Mem.* **1954**, *5*, 802.

(22) Gable, C. M.; Betz, H. F.; Maron, S. H. *J. Am. Chem. Soc.* **1950**, *72*, 1445.

(23) Bohren, C. F.; Huffmann, D. R. *Absorption and Scattering of Light by Small Particles*; Wiley: New York, 1983.

(24) Harrick, N. J. *Internal Reflection Spectroscopy*; Interscience Publishers: New York, 1967.

(25) Palmer, K. F.; Williams, D. *Appl. Opt.* **1975**, *14*, 208.

(26) Bertram, A. K.; Patterson, D. D.; Sloan, J. J. *J. Phys. Chem.* **1996**, *100*, 2376.

(27) Imre, D. G.; Xu, J.; Tridico, A. C. *Geophys. Res. Lett.* **1997**, *24*, 69.